Original Research Paper

NIR-triggered thermo-responsive biodegradable hydrogel with combination of photothermal and thermodynamic therapy for hypoxic tumor

Xiaoqi Sun[1], Di Liu[1], Xiaoyu Xu, Yifeng Shen, Yanjuan Huang, Zishan Zeng, Meng Xia, Chunshun Zhao*

School of Pharmaceutical Sciences, Sun Yat-sen University, Guangzhou 510006, China

ARTICLE INFO

ABSTRACT

Hypoxia is a typical feature of solid tumors, which highly limits the application of the oxygen-dependent therapy. Also, the dense and hyperbaric tumor tissues impede the penetration of nanoparticles into the deep tumor. Thereby, we designed a novel localized injectable hydrogel combining the photothermal therapy (PTT) and the thermodynamic therapy (TDT), which is based on the generation of free radicals even in the absence of oxygen for hypoxic tumor therapy. In our study, gold nanorods (AuNRs) and 2,2′-Azobis[2-(2-imidazalin-2-yl)propane] dihydrochlaride (AIPH) were incorporated into the hydrogel networks, which were formed by the copolymerization of hydrophobic N-isopropyl acrylamide (NIPAM) and hydrophilic glycidyl methacrylate modified hyaluronic acid (HA-GMA) to fabricate an injectable and near-infrared (NIR) responsive hydrogel. The crosslinked *in situ* forming hydrogel could not only realize PTT upon the NIR laser irradiation, but also generate free radicals even in hypoxic condition. Meanwhile the shrink of hydrogels upon thermal could accelerate the generation of free radicals to further damage the tumors, achieving the controlled drug release on demand. The designed hydrogel with a sufficient loading capacity, excellent biocompatibility and negligible systemic toxicity could serve as a long-acting implant for NIR-triggered thermo-responsive free radical generation. The *in vitro* cytotoxicity result and the *in vivo* antitumor activity illustrated the excellent therapeutic effect of hydrogels even in the absence of oxygen. Therefore, this innovative oxygen-independent platform combining the antitumor effects of PTT and TDT would bring a new insight into hypoxic tumor therapy by the application of alkyl free radical.

* Corresponding author. School of Pharmaceutical Sciences, Sun Yat-sen University, Guangzhou 510006, China.
*E-mail address:* zhaocs@mail.sysu.edu.cn (C.S. Zhao).
[1] These authors contributed equally to this work.
Peer review under responsibility of Shenyang Pharmaceutical University.

1. Introduction

Hypoxia is one of the typical characteristics of tumor microenvironment, presenting in most solid tumors [1,2]. Especially for the solid tumors in the deep tissues (>70 µm), which are far away from the nutritive blood vessels and severely hypoxic [3]. It is demonstrated that an inadequate supply of oxygen remarkably limits the efficiency of chemotherapy, radiotherapy and photodynamic therapy (PDT) [4–6]. Even many efforts have been made to elevate the oxygen level to relieve the hypoxic condition of tumor for a better therapeutic effects [7,8], but these strategies cannot solve the oxygen-dependent problem fundamentally. Fortunately, an ingenious strategy has been reported recently, which is achieved by the full use of free radicalsradicals. It has been proved that azo initiators, widely used as an initiator in the free radical polymerization reaction [9], can be decomposed rapidly under thermal stimulation [10,11], and generate the free radicals in the absence of oxygen, which could induce the lipid peroxidation and cause damage to cells [12]. This kind of oxygen-independent alkyl free radicals could be generated in large amounts even in the hypoxic tumor, which show a great potential for overcoming the limitation of the oxygen-dependent therapy especially in hypoxic tumor therapy. Because of the enhanced permeability of tumor vasculature and poor lymphatic drainage in the tumor microenvironment, nanoparticles, such as the Au nanocages [13,14], GuS [15], Nb_2C [16] were extensively utilized as carriers to deliver the alkyl free radicals for improved hypoxic tumor therapy. However, it is reported that only 0.7% of the administered nanoparticle could be delivered to a targeted solid tumor during long blood circulation [17]. The low delivery efficiency restricts the application of nanoparticles. Meanwhile the dense and hyperbaric tumor tissues impeded the delivery of nanoparticles into the deep part. Therefore, the in situ forming drug delivery systems have been developed as an alternative strategy for localized tumor therapy without systemic toxicity [18]. The localized injectable hydrogels are extremely attractive in the smart drug delivery systems due to the high drug loading capacity, excellent biocompatibility, and controlled drug release on demand upon the stimuli [19–22]. Among these stimulus, near infrared (NIR) laser is one of the attractive stimulus due to the high permeability and negligible toxicity [23]. Many photothermal conversion materials can absorb the NIR laser and efficiently convert it to heat, not only exert photothermal effect but also further stimulate the drug release on demand.

Herein, we developed a novel NIR-triggered thermal-responsive therapeutic strategy combing photothermal therapy (PTT) and oxygen-independent thermodynamic therapy (TDT) for hypoxic tumor therapy. The designed in situ hydrogel could serve as a biodegradable long-acting implant for controlled generation of free radicals to damage tumor cells even in the hypoxic condition. As demonstrated in Scheme 1, we prepared a thermo-responsive hydrogel with the crosslinking of glycidyl methacrylate modified hyaluronic acid (HA-GMA) with N-isopropyl acrylamide (NIPAM) to serve as a long-acting carrier. The alkyl free radical source 2,2′-Azobis[2-(2-imidazalin-2-yl)propane] dihydrochlaride (AIPH) and the
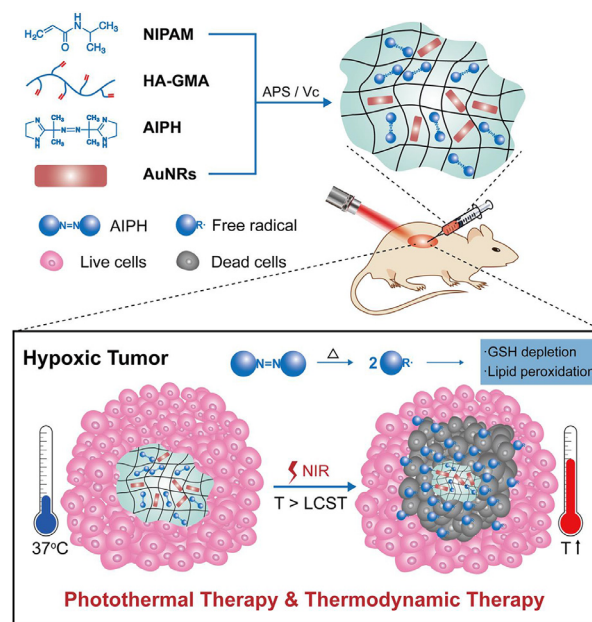
Scheme 1 – Schematic illustration of the formation of the hydrogels composed of HA-GMA and NIPAM, loaded with AIPH and AuNRs and the combination of the photothermal and thermodynamic therapy for hypoxic tumor therapy.

photothermal conversion materials gold nanorods (AuNRs) were loaded into the hydrogels during gelation process. After injection of the precursor solution intratumorally, the in situ hydrogel was formed quickly to avoid systemic toxicity. Upon the NIR laser irradiation, the AuNRs can convert the energy from the NIR laser to heat for PTT, at the same time, the thermal could trigger the generation of free radicals from AIPH for TDT even in the absence of oxygen, furthermore the shrink of hydrogel responding to heat could trigger the generation of free radicals from the hydrogel, all of which could achieve the controlled release of free radicals on demand for hypoxic tumor therapy. This localized injectable hydrogel exhibited a sufficient loading capacity, excellent biocompatibility, satisfactory biodegradable and can also realize the one single dose but multiple treatment with negligible systemic toxicity. Thus, this NIR-triggered thermo-responsive hydrogel, achieving combined PTT and TDT with the capacity of oxygen-independent free radical generation, could overcome the hypoxia limitation of the clinical tumor therapy and exhibit excellent antitumor efficiency, providing a promising potential for the treatment of hypoxic tumors.

2. Materials and methods

2.1. Materials

Sodium tetrachloroaurate ($AuCl_4Na$), diammonium 2,2′-azino-bis(3-ethylbenzothia–zoline-6-sulfonate) (ABTS), N-isopropyl acrylamide (NIPAM), and 2,2′-azobis[2-(2-imidazalin-2-yl)propane] dihydrochlaride (AIPH) were purchase from the Energy Chemical Co. Ltd (Shanghai, China). Cetyltrimethylammonium bromide (CTAB), silver

nitrate (AgNO$_3$), sodium borohydride (NaBH$_4$), glycidyl methacrylate(GMA), and fluorescein diacetate (FDA) were brought from Aladdin reagent Co. Ltd. (Shanghai, China). Ascorbic acid (Vc), ammonium persulfate (APS) and hydrochloric acid (HCl, 12 M) were obtained from SINOPHARM Chemical Reagent Co. Ltd. (Shanghai, China). Methoxypoly(ethylene glycol) thiol (mPEG-SH) with a molecular weight (MW) of 2000 was prepared by our laboratory previously. Hyaluronic acid (HA) with MW between 2×10^5—6×10^5 Da was purchased from BLOOMAGE FREDA BIOPHARM CO. LTD. (Jinan, China). 3-(4,5-dimethyl-thiazol-2-yl)−2,5-diphenyl tetrazolium bromide (MTT) and propidium iodide (PI) were obtained from Sigma-Aldrich (Shanghai, China). All reagents for the cell culture were purchased from Gibco. Deionized water was used to prepare all the aqueous solutions. All the other chemicals were analytical grade and used without further purification. 4T1 cells and MCF-7 cells were purchased from the Laboratory Animal Center of Sun Yat-sen University (Guangzhou, China).

2.2. Preparation and characterization of PEG-modified AuNRs

The PEG-modified AuNRs were synthesized as the previous method in our laboratory [24,25]. Briefly, the CTAB-coated AuNRs were synthesized by a seed-mediated growth method. Then the mPEG-SH were used to replace the CTAB to stabilize the AuNRs. The transmission electron microscope (TEM) image (TEM, JEM-1400, JEOL, Japan) and UV–vis absorption spectra (UV2600, Tianmei, Shanghai) were conducted to characterize the AuNRs. The capacity of converting the energy from NIR laser to heat was detected as follows: 1 ml AuNRs solution was irradiated with the NIR laser (785 nm, 1 W/cm^2) (Changchun New Industries Optoelectronics Technology, Changchun, China) for 10 min. The temperature was recorded in every minute by an infrared thermometer (HT-866; HCJYET, Guangzhou, China).

2.3. Synthesis and characterization of HA-GMA

HA-GMA was obtained by the reaction of glycidyl methacrylate (GMA) and hyaluronic acid under alkaline condition. Different degree of methacrylation (DM) can be obtained by adjusting the ratio of GMA to HA, and the ratio of solvent (phosphate buffer solution (PBS) and N,N-Dimethylformamide(DMF)) [26,27]. The synthetic route of HA-GMA was shown in Fig. S1. The high molecular weight (MW) macromonomer precursors hyaluronic acid (HA) with the MW between 200 and 600 kDa was selected, and the ratio of HA to GMA was determined to 1:50. The solvent was PBS/DMF (3:1). Briefly, 2 g HA was dissolved in 75 ml PBS under stirring, then 26.6 g GMA and 13.4 g TEA with 25 ml DMF were added. After stirring under 25 °C for 10 d, the solution was transferred to dialysis bags (MW:10 kDa) and dialyzed for 4 d against distilled water to remove the unreacted monomers. The dialysis fluid was changed with the fresh distilled water every 8 h. Afterwards, the white cotton like solid of HA-GMA was obtained by lyophilization for 48 h.

The chemical structure of HA-GMA was investigated with a 400 MHz NMR (AvanceIII, Bruker, Switzerland) by using TMS

Table 1 – The compositions of poly(HA-GMA-co-NIPAM) hydrogels.

Sample	HA-GMA:NIPAM (mg/mg)	HA-GMA (mg)	NIPAM (mg)	5%APS (µl)	5%Vc (µl)
HAN-1	1:4	10	40	50	50
HAN-2	1:2	10	20	50	50
HAN-3 (GEL(Blank))	1:1	10	10	50	50
HAN-4	2:1	10	5	50	50
HAN-5	4:1	10	2.5	50	50
HAN-6	1:1	10	10	10	10
HAN-7	1:1	10	30	30	30
HAN-8	1:1	10	70	70	70

Table 2 – The compositions of poly(HA-GMA-co-NIPAM)/Au-NR/AIPH hydrogels.

Sample	HA-GMA:NIPAM (mass ratio, mg/mg)	AuNR (ug)	AIPH (mg)	5%APS (µl)	5%Vc (µl)
GEL(Au)	1:1(10mg:10 mg)	100	0	50	50
GEL(AIPH)	1:1(10mg:10 mg)	0	2	50	50
GEL(Au+AIPH)	1:1(10mg:10 mg)	100	2	50	50
GEL(Control)	1:0(20mg:0 mg)	100	2	50	50

as an internal standard. Deuterium oxide (D$_2$O) was used as the solvent. The double bonds attributed to the modification of HA with GMA were confirmed by Fourier Transform Infrared spectrometer (FTIR, Spectrum Two, PerkinElmer, USA) equipped with an Attenuated Total Reflectance (ATR) accessory.

2.4. In vitro hydrogel preparation

The cross-linking reaction between the HA-GMA and NIPAM was initiated under the APS/Vc redox system through the polymerization of double bonds on each monomer. The appropriate formula of the hydrogel composed of HA-GMA and NIPAM should be screened. Briefly, 10 mg of HA-GMA was mixed with different weight of NIPAM (40 mg, 20 mg, 10 mg, 5 mg, 2.5 mg) and dissolved in 200 µl distilled water, as shown in Table 1. APS and Vc were selected as the initiator to trigger polymerization. Considering that the quantity of APS and Vc would influence the rate of the polymerization and systemic toxicity to cells, different volume of 5% APS (w/w) and 5%Vc (w/w) (10 µl, 30 µl, 50 µl, 70 µl) were added to the precursor mixture solutions and the ultimate volume was fixed at 0.5 ml by adding distilled water. After violent vortex, the mixture was transferred to a 2 ml syringe. The formation of hydrogel was carried out at the room temperature(25 °C) and physiological temperature (37 °C) to simulate the room temperature and physiological temperature respectively. The gelation time was based on the vial inverting method [28]. The AuNRs and AIPH-loaded hydrogels were conducted as the same procedures, by mixing the AuNRs or AIPH with the precursor solutions additional, as shown in Table 2. Besides, in the control group (GEL(Control)), the NIPAM was replaced with hydroxyethyl methacrylate (HEMA) with similar hydrophobic and

hydrophobic properties but no thermal responsibility to serve as a hydrogel without the function of shrink under thermal.

2.5. Characterization of hydrogels

2.5.1. Swelling behavior of the thermo-responsive hydrogels
Different composition of hydrogels have different sensitivity to heat, in order to investigate the thermal property of the hydrogels, the gravimetric method was used to evaluate the equilibrium swelling ratio of the hydrogel [29]. Firstly, the hydrogels with different weight ratios of HA-GMA/NIPAM (1:4, 1:2, 1:1, 2:1, 4:1) were prepared as above and lyophilized, the weight of the dried hydrogels was designated as Wd. Then lyophilized hydrogels were swelled sufficiently by an excess of pure water for 48 h in different temperatures from 25 to 50 °C. After wiping up the surface of the samples with filter paper, the weight of hydrogels after swelling was recorded as Ws. Take the average value of three times of each sample. The equilibrium swelling ratio (Se), was determined as follows:

$$Se\ (\%) = (Ws - Wd)/Wd \times 100\%$$

2.5.2. The rate and the efficiency of gelation
The gelation time of hydrogels was determined by the inverted tube test. Different quantity of the initiator was utilized when preparing hydrogels. The gelation time of the as-prepared hydrogels (HAN-3(GEL(Blank)), HAN-6, HAN-7, HAN-8) were recorded under the room temperature(25 °C) and physiological temperature (37 °C), respectively. The efficiency of the gelation was defined as the ratio of the weight of lyophilized hydrogel to the total weight of materials composed of hydrogels. Parallel five hydrogels of HAN-3 were prepared and lyophilized after immersed for 24 h in the water, recorded the weight of dried hydrogels. Calculate the ratio of weight of dried hydrogels to the weight of materials and obtain the average efficiency of gelation.

2.5.3. Rheological measurements
The mechanical strength of the as-prepared hydrogels (GEL(Blank) and GEL(Au)) was evaluated by rheological measurement using Kinexus Pro rheometer (Malvern Instruments Ltd., Worcestershire, UK) with the 25 mm-diameter parallel plate [25]. The hydrogels were placed on the plate with the gap of 1 mm at 25 ± 0.1 °C. Frequency-sweep tests at constant strain of 5% were carried out over the frequency range of 0.1 to 100 Hz to obtain the storage modulus (G') and loss modulus (G'') of hydrogels.

2.5.4. Morphology characterization of the hydrogels
The microstructures of lyophilized hydrogels were analyzed by Scanning-Electron-Microscope (EVO SEM, EVO MA10, Carl Zeiss AG). The sample of HAN-3(GEL(Blank)) was swelled sufficiently followed by lyophilized for 48 h and then fixed on aluminum plates and coated with gold. Moreover, the structure of hydrogels was measured by FTIR equipped with ATR accessory.

2.5.5. NIR-Stimulated thermo-responsive property tests
To investigate the thermo-responsive behaviors of the hydrogels with the AuNR, the swollen hydrogel(GEL(Au)) was exposed to a 785 nm NIR laser at power densities of $1 W/cm^2$. The photographs at different irradiation time (1 min, 2 min, 3 min, 4 min, 5 min) were taken and the weight of hydrogels at corresponding was also recorded. After irradiation, hydrogels were immersed in pure water again to reswell for 2 h. The blank hydrogel (HAN-3) was selected as control.

2.5.6. In vitro free radicals detection and the generation of free radicals in response to NIR irradiation
ABTS was utilized to characterize the generation of free radicals of AIPH. The ABTS could capture the free radicals generated from AIPH, and the generated $ABTS^{+\cdot}$ exhibited a characteristic absorbance between 500 and 900 nm [13,14]. To verify the thermo-sensitivity of AIPH, the mixture of ABTS (0.2 mg/ml, 0.2 ml) and AIPH (2 mg/ml, 0.2 ml) was cultured at 45 °C in water bath in the dark. The absorbance of the mixture from 0 to 15 min between the wavelength of 500 to 900 nm was recorded using a UV–Vis spectrometer. Afterwards, to demonstrate the generation of free radicals of AIPH, the hydrogels of GEL(AIPH) and GEL(Au+AIPH) were cut into two equal piece and put into the solution of ABTS (0.2 mg/ml, 2 ml) respectively. One of the solution was irradiated with NIR laser at 785 nm with $1 W/cm^2$, and the other was kept in the dark as control, the UV–Vis absorbance spectra of solutions between 500 and 900 nm were recorded at different time (0 min, 5 min, 10 min, 15 min). To evaluate the NIR responsiveness of the generation of free radicals of AIPH, hydrogels of GEL(AIPH), GEL(Au+AIPH) and GEL(Control) were respectively immersed in the solution of ABTS (0.2 mg/ml, 2 ml) and exposed to the NIR irradiation (785 nm, $1 W/cm^2$) for 5 min. Then the solution was kept in the dark for 1 h, the UV absorption of the solution at 736 nm was measured. Similarly, this operation was repeated for another four cycles to record the changes of UV absorption of the solution, which could reflect the generation of the free radicals of AIPH with or without the laser irradiation.

2.5.7. In vitro degradation of hydrogels
The degradation of the hydrogels was measured according to the weight loss in PBS in the presence of hyaluronidase [30,31]. The hydrogels of HAN-3 were inserted into 6 ml PBS containing different concentration of hyaluronidase (0, 5 U/ml, 50 U/ml, 100 U/ml) at 37 °C in the shaker. At specified time intervals, hydrogels were taken out and weighed and transferred into the fresh hyaluronidase solutions subsequently. The measurements were continued to 15 d

2.5.8. In vitro depletion of glutathione
Free radicals generated from AIPH can consume the antioxidants like Glutathione, the assay of glutathione was based on the reaction of GSH with 5,5ʹdithiobis-(2-nitrobenzoic) acid (DTNB) [32,33]. The hydrogel of GEL(Au+AIPH) was added into the reaction solution contained 100 μM GSH and 125 μg/ml DTNB with total volume of 2 ml. Then the hydrogel was irradiated with NIR laser (785 nm with $1 W/cm^2$) for 30 min, and the UV–Vis absorbance of solutions at 412 nm were recorded at specified time intervals with or without irradiation. The mixture solution without hydrogel were served as blank control with or without irradiation

2.6. In vitro cellular assay

2.6.1. Cytotoxicity evaluation of hydrogels

Firstly, 4T1 cells and MCF-7 cells were cultured at 37 °C in a 5% humidified CO_2 incubator in DMEM or PRMI-1640 culture medium supplemented with 10% fetal bovine serum and 1% penicillin/streptomycin respectively. The effect of hyperthermia and the free radicals on the cancer cells was examined by MTT assay. Briefly, 4T1 cells and MCF-7 were plated on a 12-well plate with the density of 1×10^5 cells/well and cultured in incubator for 24 h. Then, transwell inserts with the hydrogels of GEL(Au), GEL(AIPH), GEL(Au+AIPH) as prepared in Table 2 were placed on the wells with the total medium of 1.5 ml per well. Next, the cells were irradiated with NIR laser irradiation (785 nm, 1 W/cm^2) for 10 min. Then the cells were cultured for another 24 h. Cells without hydrogels were taken as control group, also the groups of cells without irradiation were treated as the same. And for the hypoxia groups, the culture medium was contained 100 µM $CoCl_2$ additionally. At last, the cells were incubated with additional 150 µl MTT solution for another 4 h, then the medium was replaced with 1.5 ml DMSO followed by shaking for 15 min, and the optical density (OD) of each well was measured at 490 nm by microplate reader (ELX800, Bio-Tek, USA). The cell viability was determined as the ratio of OD value of treated wells to the OD value of control group.

2.6.2. Intracellular free radical generation detection

DCFH-DA was selected as the indicator of intracelluar free radicals from AIPH. 4T1 cells were seeded on the cell slides in the 12-well plate with the density of 1×10^5 cells per well and incubated for 24 h. Firstly, the cells was pre-incubated with DCFH-DA solution (10 µM, 500 µl) for 30 min, and washed with PBS for three times, and replaced with the fresh medium. Then, transwell inserts with the hydrogels of GEL(Au), GEL(AIPH), GEL(Au+AIPH) were placed on the wells with the total medium of 1.5 ml per well. Afterwards, the cells were irradiated with NIR laser (785 nm, 1 W/cm^2) for 10 min with the laser spot of 1 cm in diameter or in the dark. Afterwards, the cells slides were fixed with 4% paraformaldehyde for 10 min, followed by stained with DAPI. The intensity of green fluorescence was obtained by laser scanning confocal microscope (FV3000, Olympus, Japan) at an excitation at 488 nm. For the hypoxia groups, the culture medium was contained 100 µM $CoCl_2$ additionally.

2.6.3. Intracellular depletion of glutathione

The intracellular glutathione level was detected by the commercial GSH assay kit (Solarbio, Beijing, China) [34]. 4T1 cells were seeded in the 12-well plate with the density of 1×10^5 cells per well and incubated for 24 h. Then, transwell inserts with the hydrogels of GEL(Au+AIPH) were placed on the wells with the total medium of 1.5 ml per well. The cells were irradiated with NIR laser (785 nm, 1 W/cm^2) for 10 min with the laser spot of 1 cm in diameter. Then the cells were cultured for another 24 h. Afterwards, each well was washed with PBS for three times, suspended in PBS, and centrifuged at 600 g for 10 min. Then, the cells were frozen and thawed for two cycles and centrifuged at 8000 g for 10 min at 4 °C. After

that, 20 µl of supernatant was added to the testing solution in an assay kit and co-incubated for 2 min and measured by UV–vis spectroscopy at a wavelength of 412 nm. For the hypoxia groups, the culture medium was contained 100 µM $CoCl_2$ additionally.

2.6.4. Intracellular lipid peroxidation detection

The intracellular lipid peroxidation level was measured base on the reaction between malondialdehyde (MDA) and thiobarbituric acid (TBARS) [35]. The 4T1 cells after treated with hydrogels of GEL(Au+AIPH) under irradiation (785 nm, 1 W/cm^2, 10 min) were lysed with the lysis solution and centrifuged at 12 000 g for 10 min at 4 °C. The supernatant was collected and used for analyzing with the Lipid Peroxidation MDA assay kit (Beyotime, Jiangsu, China). The relative MDA level was determined as the percentage of the UV–Vis absorbance at 532 nm over the absorbance of the control group. For the hypoxia groups, the culture medium was contained 100 µM $CoCl_2$ additionally.

2.7. In vivo evaluations of hydrogels

2.7.1. In vivo gel formation and biocompatibility

BALB/C mice (4–6 weeks) were provided by the Laboratory Animal Center of Sun Yat-sen University (Guangzhou, China). All animal experiments were conducted following the guidelines of laboratory animals supervised by the Institutional Animal Care and Use Committee of Sun Yat-sen University. To verify the feasibility of gelation in vivo, 200 µl of the precursor solution of GEL(Au+AIPH) was injected into the back of BALB/C mice subcutaneously. After 10 min, the mice were euthanized and the picture was taken on the injection site. The mice were sacrificed at the 48th d after injection to evaluate the long-term toxicity. The major tissues (heart, liver, spleen, lung, kidney, skin and muscle) were dissected and fixed, then stained with hematoxylin-eosin (H&E) and observed.

2.7.2. In vivo antitumor activity of hydrogels

The BABL/C mice bearing 4T1 xenograft model were established by injecting suspension of 4T1 cells (1×10^7 cells/ml, 100 µl) subcutaneously on the back of each mice. When the volume of tumor was reached to 100 mm^3, these mice were randomly divided into eight groups ($n = 5$) : (1) Saline: intratumorally injected with saline, (2) Saline (IR): intratumorally injected with saline with irradiation at the specific time , (3) GEL(Au): intratumorally injected with precursor solution of GEL(Au), (4) GEL(Au) (IR): intratumorally injected with precursor solution of GEL(Au) with irradiation at the specific time , (5) GEL(AIPH): intratumorally injected with precursor solution of GEL(AIPH), (6) GEL (AIPH) (IR): intratumorally injected with precursor solution of GEL(AIPH) with irradiation at the specific time, (7) GEL(Au+AIPH): intratumorally injected with precursor solution of GEL(Au+AIPH), (8) GEL(Au+AIPH) (IR): intratumorally injected with precursor solution of GEL(Au+AIPH) with irradiation at the specific time. Each group was injected with corresponding precursor solution of 200 µl. For the groups of irradiation (2,4,6,8), the mice were anesthetized and implemented with the NIR laser

irradiation (785 nm, 1 W/cm^2,10 min) at the 1, 3, 5, 7, 9, 11, 13, 15, 17 and 19 d after injection. The body weights and volumes of tumor were measured and recorded everyday over a period of 24 d The volume of tumor was defined as: V= (tumor length) × (tumor width)^2/2. At the end of therapy, all the mice were sacrificed, and the tumors were excised and photographed. The tissues in the group of GEL(Au+AIPH) (IR) were also excised, followed by fixed and sliced for H&E staining for histopathological assay to verify the safety of the hydrogels after therapy.

2.7.3. In vivo IR thermal images of hydrogels

The 4T1 tumor-bearing mice were intratumorally injected with 200 ul Saline, precursor solution of GEL(Au)and GEL(Au+AIPH). The mice were applied with the NIR laser irradiation (785 nm, 1 W/cm^2) for 5 min and 10 min [36]. The temperature of tumor was measured by the IR thermal camera (FLUKE, Ti27). The same operation was also implemented at the Day 3 and 5 to record the photographs of mice (785 nm, 1 W/cm^2, 10 min).

2.7.4. In vivo degradation of hydrogels

To verify the biodegradation of the hydrogel in vivo, 200 µl of the precursor solution of GEL(Au+AIPH) was injected subcutaneously into the back of the BABL/C mice. The mice were euthanized at 1, 24 and 48 d after injection. The position of in-situ gelation was examined by a digital camera. The photographs at different days were taken as record.

2.8. Statistical analysis

All the data were given as mean ± standard deviation (SD). One way analysis of variance was used to determine the significance of the difference. The differences were considered significant for *P < 0.05, **P < 0.005, ***P < 0.0005 or ****P < 0.0001.

3. Results and discussion

3.1. Preparation and characterization of PEG-modified AuNRs

The PEG-modified AuNRs were prepared by the previous method [24]. mPEG-SH was selected to modify the AuNRs by a ligand exchange reaction to diminish the cytotoxicity and enhance the biocompatibility. The prepared AuNRs were characterized by the TEM images and UV–Vis spectrum. As shown in Fig. 1A, the AuNRs showed the average length of 50 nm and average width of 12 nm. Moreover, the AuNRs exhibited a longitudinal surface plasmon resonance band at around 790 nm in the NIR region in Fig. 1B. There was no significant difference between the CTAB-coated AuNRs and PEG-coated AuNRs in the UV–Vis absorption spectrum. The photothermal conversion capacity of AuNRs was verified as shown in Fig. 1C, the solution of AuNRs can convert NIR laser into heat and cause the obvious elevation of temperature upon irradiation which exhibited a great potential for tumor hyperthermia therapy and TDT.

3.2. Synthesis and characterization of HA-GMA

HA-GMA was synthesized by conjugating GMA with the HA under alkaline condition as shown in Fig. S1. A reversible transesterification was conducted through the ring-opening reaction between the primary hydroxyl group of HA and the epoxy group of GMA. The degree of methacrylation (DM) can be adjusted by the ratio of HA to GMA, the solvent and the reaction time. The 1H NMR spectrum of the HA-GMA analyzed in D$_2$O was shown in Fig. 2A (the amplified images was shown in Fig. S1B). The typical methacrylate peaks of protons of double bonds and methyl group were designated at 6.13 ppm, 5.72 ppm, and 1.90 ppm. The DM defined as the amount of methacryloyl groups per HA disaccharide repeat unit was calculated from the ratio of the relative peak integration of the methyl protons of methacrylated (peaks as 1.90 ppm) to the methyl protons of HA (peaks at 1.97 ppm). The degree of methacrylation was about 37.5%, which meant that there were enough double bonds on the HA-GMA monomer chains to crosslink with the double bonds on the NIPAM monomer to obtain a dense hydrogel, which could meet the requirement for the further application.

3.3. In vitro characterization of hydrogels

3.3.1. Swelling behavior of the thermo-responsive hydrogels

The poly-NIPAM (PNIPAM) is a kind of thermo-responsible macromolecule with the lower critical solution temperature LCST at 32 °C and exhibits a temperature-dependent phase transition in aqueous solution at its LCST, leading to changes of its hydrophobic/hydrophilic properties [37]. The typical characteristic of PNIPAM is that its hydrophily will change with the temperature. When the temperature is low, the hydrogen-bond interactions between the monomer of NIPAM endow the hydrophily of the structure. However, the hydrogen-bond interactions will be weakened with the increase of temperature, when the temperature was above LCST, the hydrogel of PNIPAM would show a sharp shrink. LCST of PNIPAM is too low to be utilized in the biological materials and need to be adjusted by changing the composition of the monomer [38,39]. When the ratio of the hydrophilic monomer is increased, LCST would be increased as well. So, we mixed the hydrophilic monomer HA-GMA to copolymerize with NIPAM to increase LCST [40]. As shown in Table 1, different ratio of HA-GMA to NIPAM was prepared to obtain the hydrogels. And all the hydrogels with different composition were determined to obtain the appropriate LCST to satisfy the needs of the good biocompatibility and controlled drug delivery through the thermo-responsive swelling behavior. It can be seen that LCST of hydrogel was elevated with the increase ratio of hydrophilic monomer HA-GMA in Fig. 2B. When the ratio of HA-GMA to NIPAM was 1:1, LCST of the hydrogel was about 39 °C, which was a little higher than the physiological temperature 37 °C, and a little lower than the temperature of tumor hyperthermia 40–45 °C, which meant that the hydrogel would be swollen at physiological state and a sharply shrunken at the hyperthermia to obtain the controlled drug delivery. So
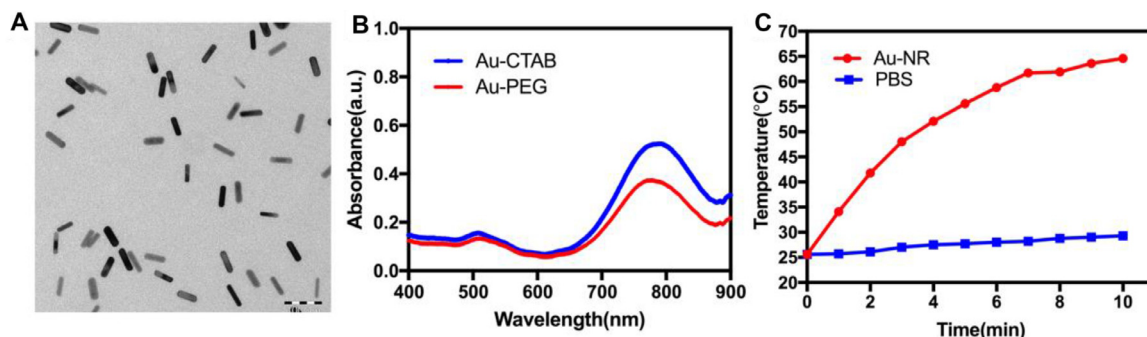
Fig. 1 – (A) TEM images of PEG-coated gold nanorods (AuNRs). Scale bar:100 nm. (B) UV–Vis absorbance of Au-CTAB and Au-PEG in deionized water. (C) Temperature change of Au-NR and PBS under NIR laser irradiation (785 nm, 1 W/cm^2).
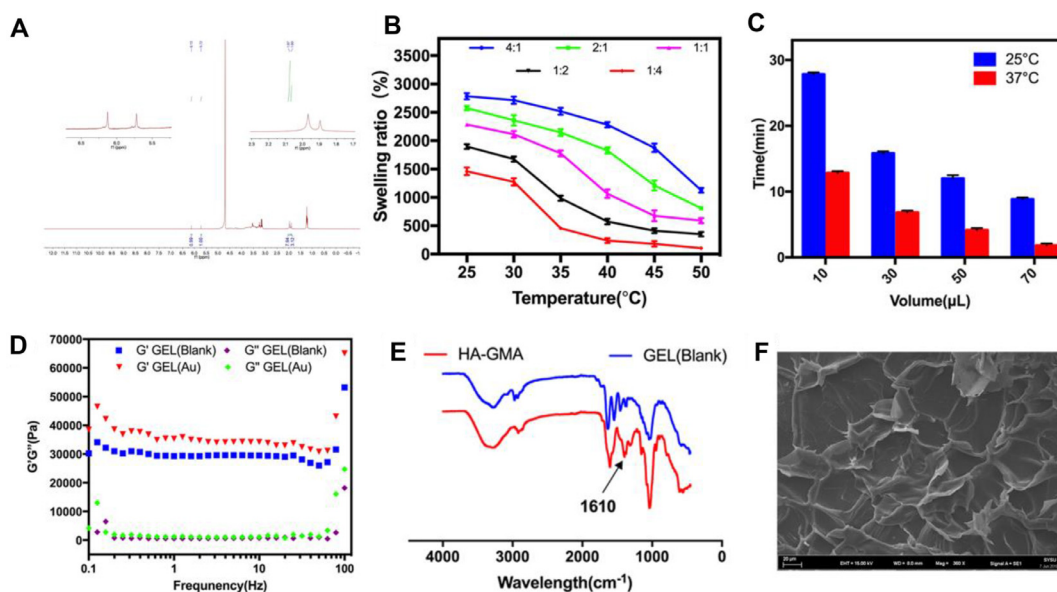

Fig. 2 – Characterization of hydrogels. (A) ^{1}H NMR spectrum of HA-GMA in D$_2$O. (B) Swelling rations of different composition (HA-GMA: NIPAM) of hydrogels. (C) The rate of gelation in 25 and 37 °C with different amount of initiators of blank gels. (D) Frequency dependency of the storage modulus (G') and loss modulus (G'') of GEL(Au) and GEL(Au+AIPH). (E)FT-IR spectra of HA-GMA and GEL(Blank). (F) SEM images of GEL(Blank) with scale bar 20 μm.

the hydrogels with a ratio of HA-GMA to NIPAM of 1:1 were selected for the further study.

### 3.3.2. The rate and the efficiency of gelation

The APS and Vc redox system were selected as the initiator to trigger polymerization of the double bonds of the HA-GMA and NIPAM as previous method [24]. The amount of the initiators would influence the rate of gelation. The gelation time was based on the vial inverting method. As shown in Fig. 2C, the gelation time was decreased with the increase of the amount of initiators, and the gelation rate was improved at 37 °C than at 25 °C respectively. When the volume of 5% APS (w/w) and 5% Vc (w/w) was 50 μl, the gelation time was 12 min at 25 °C and 4.5 min at 37 °C respectively, which not only can provide a sufficient time to inject subcutaneously at room temperature but can become a gel like stated quickly in physiological environment to avoid the flow of the solution. So there was enough time for precursor solution of hydrogel mixing sufficiently in vitro, and after injection, the gelation

could be formed quickly in vivo to avoid the loss of monomer. The efficiency of gelation was calculated by the mass ratio of dried hydrogels to the materials used. The average efficiency of gelation was 98.5% ± 0.08%, which meant that almost all the monomer was polymerized and the cytotoxicity of monomer was diminished. Moreover, the rate of gelation was fast in the physiological environment, which could also diminish diffusion of the monomer with a decreased toxicity. As shown in Table 2, for GEL(Au+AIPH), the loading capacity of AuNRs was 0.5 mg/ml, and the loading capacity of AIPH was 9.05%.

3.3.3. Rheological characterization and FT-IR spectra of hydrogel

The viscoelastic properties of hydrogels were characterized by rheological measurements. As shown in Fig. 2D, both of hydrogels had the similar viscoelastic properties, indicating that AuNRs had negligible influence on the viscoelastic properties of hydrogels. For both of GEL(Au) and HAN-3(GEL(Blank)), the value of storage modulus (G') was
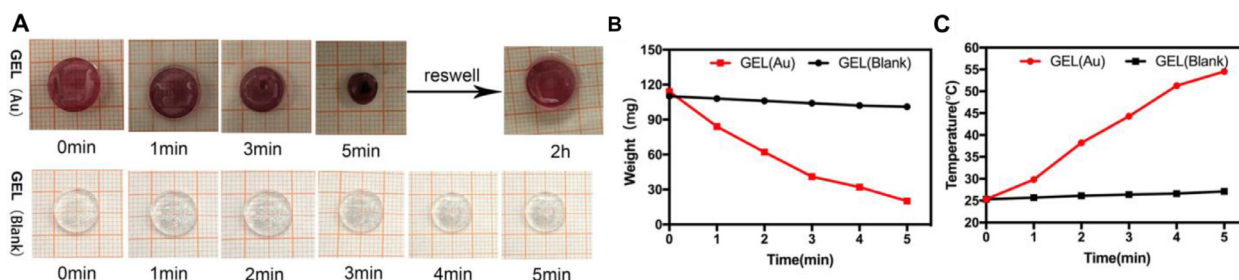
Fig. 3 – NIR-triggered thermo-responsive property of hydrogels. (A) Photographs of the GEL(Au) and GEL(Blank) at different time with NIR laser irradiation (785 nm, 1 W/cm^2) for 5 min, and reswollen in deionized water after 2 h. (B) Weight changes of GEL(Au) and GEL(Blank) during irradiation. (C) Temperature changes of GEL(Au) and GEL(Blank) during irradiation.

considerably higher than the value of loss modulus (G'') over the change of frequency, indicating that the hydrogels exhibited the high elasticity with the strong mechanical strength. When the value of storage modulus (G') was higher than the value of loss modulus (G''), the materials exhibited more properties of gel rather than sol, so the hydrogels prepared were possessed of good mechanical stability and high mechanical strength for prolonged retention time intratumorally. Moreover, the crosslinked covalent bonds between the HA-GMA and NIPAM formed the hydrogels were determined by FTIR spectra in Fig. 2E, which confirmed that the double bonds (1610 cm^{-1}) of the HA- GMA were almost disappeared after crosslinking with NIPAM, suggesting that the hydrogels were synthesized by the crosslink of the double bonds of the HA-GMA and NIPAM.

3.3.4. Morphology characterization of the hydrogels

The interior morphologies of the hydrogels were characterized by the SEM in Fig. 2F with scale bar of 20 μm, confirming the porous structure of hydrogels. The well-defined porous network structure of the lyophilized hydrogels was attributed to the high-water content in the hydrogels, which was beneficial to load the AuNRs and drugs. When the hydrogels were sharply shrunken under thermal, the loaded drugs in the pores would be squeezed out along with the water to realize the controlled drug release.

### 3.3.5. NIR-Stimulated thermo-responsive property tests

The NIR-stimulated thermo-responsive behavior of hydrogels was investigated by irradiating the GEL(Blank) and GEL(Au) with a NIR laser of wavelength of 785 nm at a power of 1 W/cm^2. Because of the photothermal conversion ability of AuNRs, GEL(Au) would show a significant absorption for the NIR laser and convert the laser to the thermal, which would lead to a dramatically shrunk and a strong warming of hydrogels, exhibiting the thermo-responsive properties of the PNIPAM-based hydrogels. After irradiation, the collapsed hydrogel could reswell to an elastic state in the deionized water. As illustrated in Fig. 3A, upon the irradiation for 5 min, the hydrogel of GEL(Au) could shrank significantly, the volume was decreased dramatically, and the weight of the hydrogel was also decreased as demonstrated in Fig. 3B. AuNRs can absorb the energy from NIR laser and convert it to heat, resulting in the increased temperature of hydrogels, shown in Fig. 3C. Once the temperature was increased above the LCST of

the hydrogels, the hydrogels would show a significant shrink and lead to the squeeze of the water along with the decrease of volume and the weight of hydrogels. On the contrary, the hydrogel of GEL(Blank), which contained no AuNRs, wouldn't show the obvious elevation of temperature and the decrease of volume and weight. Interestingly, after irradiation, the temperature was descended, the hydrogel of GEL(Au) could be completely reswollen to the original state in the deionized water after 2 h in the room temperature. The responsiveness of the hydrogels to NIR demonstrated that the hydrogels exhibited excellent photothermal properties and contraction upon heat as well as reversible recovery.

3.3.6. In vitro free-radical detection and the generation of free radicals in response to NIR irradiation

The free radicals generated by AIPH can be measured by ABTS, which can react with the AIPH+·, and generate the free radical of ABTS (ABTS+·), with a characteristic absorbance in the wavelength of 500 to 900 in the UV–Vis spectra. The production of ABTS+· could reflect the generation of free radical from AIPH. The generation of free radicals of AIPH was measured in the presence or the absence of the NIR laser irradiation (785 nm, 1 W/cm^2) with or without AuNRs. Firstly, as illustrated in Fig. S2, the water solution of AIPH (2 mg/ml) in the presence of ABTS (0.2 mg/ml) was incubated in the 45 °C water bath for 15 min, the characteristic absorbance in the ranging of 500 to 900 were increased with the incubation time, suggesting the production of ABTS+· under heat, which indicated the generation of AIPH+·. In the similar way, when put the hydrogels into the solution of ABTS, and the NIR laser was exerted to the hydrogels, the characteristic absorbance of UV–Vis spectra of GEL(Au+AIPH) were also observed that the obvious time-dependent generation of ABTS+· after irradiation for 15 min in Fig. 4A, but there was almost no ABTS+· without irradiation in Fig. 4B. Although AIPH was small water-soluble molecule with positive charge, which would be a challenge for its delivery due to the pre-leakage. However, Compared with Fig. 4A and 4B, only about 4.5% AIPH+· was generated and released because of diffusion in the total amount of released AIPH+· under irradiation, indicating the diminished leakage of AIPH and NIR could trigger the generation of the AIPH+· on demand. Since the principal constituent of the hydrogel was modified hyaluronic acid macromolecular chains with plenty of negative charges, which may could induce the huge electrostatic absorption
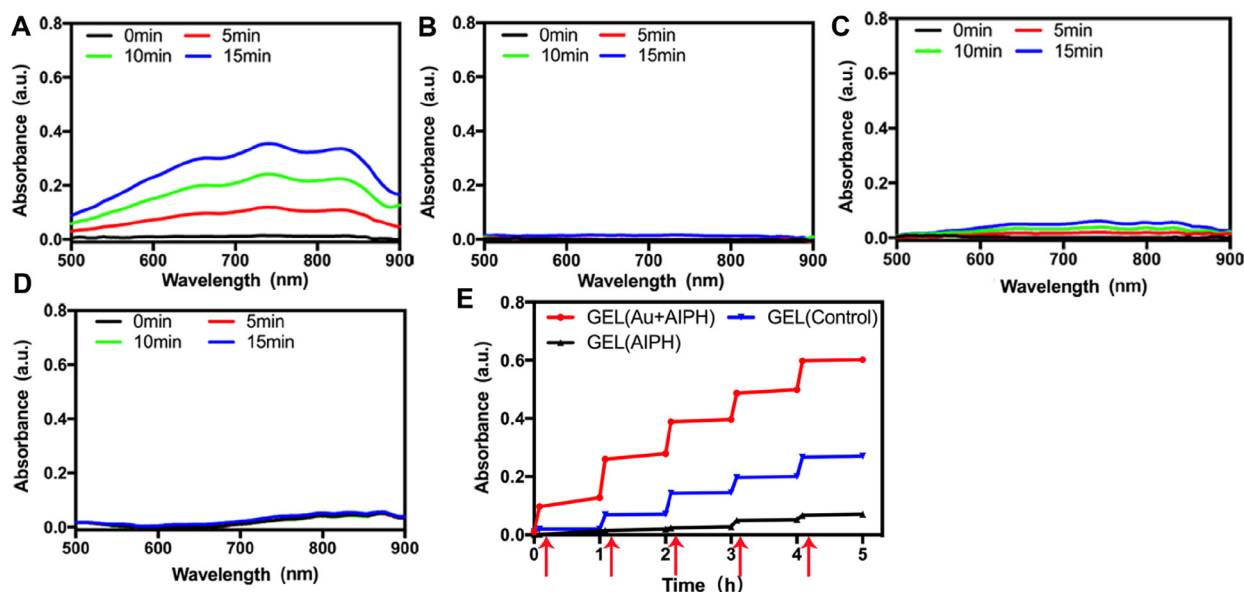
Fig. 4 – Detection of the generation of free-radical _in vitro_. UV–Vis spectrum of radical detection (A) The UV–Vis spectra of ABTS solution contained GEL(Au+AIPH) with irradiation (785 nm, 1 W/cm^2). (B) The UV–Vis spectrum of ABTS solution contained GEL(Au+AIPH) without irradiation. (C) The UV–Vis spectrum of ABTS solution contained GEL(AIPH) with irradiation (785 nm, 1 W/cm^2). (D) The UV–Vis spectrum of ABTS solution contained GEL(AIPH) without irradiation. (E) The absorbance changes of the solution of ABTS solution contained GEL(AIPH), GEL(Au+AIPH) and GEL(Control) with or without irradiation at given time. Five cycles of NIR irradiation with 785 nm, at the power of 1 W/cm^2 for 5 min at 0, 1, 2, 3, 4 h and dark for 1 h.

effect with the AIPH. So through the electrostatic absorption, van der Waals forces, and hydrogen bonding, the AIPH could be loaded into the hydrogels with a decreased leakage. What's more, when there was no AuNRs in the hydrogels such as GEL(AIPH), neither in the presence nor the absence of the irradiation, there was nearly no significant AIPH+· release, because the temperature couldn't be risen obviously without AuNRs as shown in Fig. 4C and 4D. All these results illustrated that the free radical of AIPH in the hydrogel of GEL(Au+AIPH) could be released under irradiation and nearly no leak without irradiation, which exhibited the good biocompatibility and on-demand release of AIPH+·.

The generation of free radicals of AIPH in response to the NIR laser irradiation was detected by the changes of the UV absorption of ABTS solution at 736 nm as shown in Fig. 4E. Upon the NIR laser, which could be absorbed by the AuNRs in the hydrogels and converted it to the heat, resulting in the generation of free radicals of AIPH, the GEL(Au+AIPH) contained AuNRs in the hydrogel could significantly generate the free radicals of AIPH compared with GEL(AIPH), which contained no AuNRs. Upon the irradiation for 5 min, the free radicals could be generated and when kept the hydrogels in the dark, there was nearly no free radicals generating, indicating the controlled generation of free radicals on demand. Moreover, to verify the shrink of the hydrogels by the heat of AuNRs upon irradiation could accelerate the release of the generated free radical. The hydrogel of GEL(Control), which contained the AuNRs but used HEMA replaced the NIPAM, only exhibited the ability of photothermal effect but no shrink behavior under irradiation. As seen in Fig. 4E, the hydrogel of GEL(Control) could generate

the free radicals upon irradiation, but the level of the free radicals was less than GEL(Au+AIPH), which could be shrunk under thermal upon irradiation and further accelerate the release of the free radicals. Excitingly, the cycles could be repeated between the irradiation and dark condition, which confirmed the long-acting effect and the multiple treatment at single dose.

3.3.7. In vitro degradation and depletion of glutathione of hydrogels

Hyaluronidase existed in many tissues, especially in the body fluids, which could degrade the hyaluronic acid. To confirm the hydrogels would not be prevented degradation by hyaluronidase, the GEL(Blank) were immersed in the PBS containing different concentration of hyaluronidase (0, 5 U/ml, 50 U/ml, 100 U/ml) at 37 °C in the shaker. The degradation was measured with respect to the weight loss under various concentration of hyaluronidase solution. As demonstrated in Fig. S3A, the hydrogels with high concentration of hyaluronidase degraded faster than low concentration of hyaluronidase. For the hyaluronidase of 100 U/ml, the hydrogels could fully be degraded in 8 and 14 d for the hyaluronidase of 50 U/ml. However, for hyaluronidase of 5 U/ml and the PBS without hyaluronidase, the hydrogels showed a slow degradation rate, and had no obvious change under 16 d, only show a slight loss of weight. As for the hyaluronidase with 50 U/ml, the degradation kinetics of the hydrogels was tested using the zero-order model and first-order models by the non-linear least square, the results showed that the kinetics of the degradation in vitro was better described with zero-order kinetics with the degradation
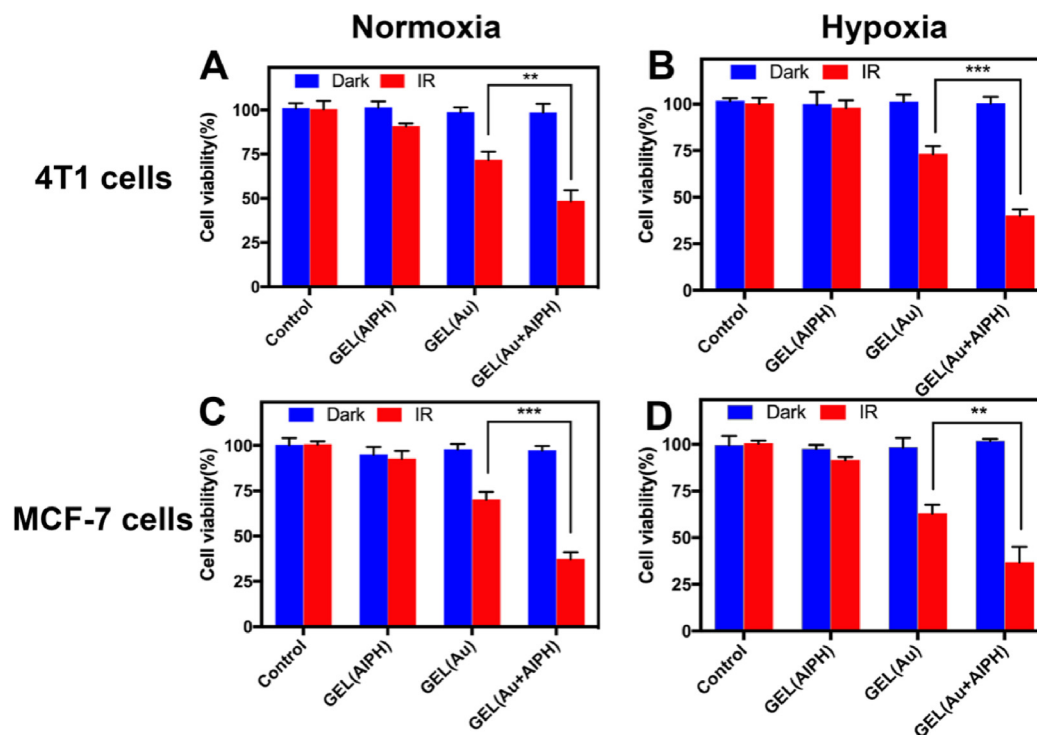
Fig. 5 – Cytotoxicity Evaluation of Hydrogels under normal oxygen concentration and hypoxia condition. Cell viability of 4T1 cells treated with hydrogels with or without irradiation (785 nm, 1 W/cm^2,10 min) (A) under normal oxygen concentration, (B) under hypoxia condition. Cell viability of MCF-7 cells treated with hydrogels with or without irradiation (785 nm, 1 W/cm^2, 10 min) (C) under normal oxygen concentration, (D) under hypoxia condition. ($n = 3$, **$P < 0.005$, ***$P < 0.0005$).

kinetic profile as follows:

$$W(mg) = 587.86 - 83.65 \times T$$

W was represented as the mass of the hydrogels, and T was represented as the degradation time (day).

Similarly, for the hyaluronidase with 100 U/ml, the degradation kinetics of hydrogels was also ascribed to the zero-order kinetics with the degradation kinetic profile of $W(mg) = 700.83 - 175.5 \times T(d)$. And for the hyaluronidase with 5 U/ml, the degradation kinetics of hydrogels was also ascribed to the zero-order kinetics with the degradation kinetic profile of $W(mg) = 351.28 - 10.14 \times T(d)$.

Glutathione (GSH), served as a representative antioxidant, plays an important role in the oxidation–reduction system. It is assumed that the generation of free radical from hydrogels under irradiation could consume the GSH, causing the depletion of GSH, which would break the redox balance. To verify the hypothesis, the level of GSH was examined in the DTNB solution. As shown in Fig. S3B, the relative level of GSH was dramatically decreased for hydrogel of GEL(Au+AIPH) under the NIR laser irradiation (785 nm, 1 W/cm^2) for 30 min compared with the dark condition, confirming the remarkable GSH consumption ability of the AIPH+·, which could further break the redox balance and cause damage to cells.

3.4. *In vitro cellular assay*

3.4.1. *Cytotoxicity evaluation of hydrogels*
Having proved the photothermal effect and the generation of free radical of the hydrogels in the solution, in the next step, we examined the therapeutic effect to cells through a standard MTT assay. To verify the combination of the photothermal and thermodynamic therapeutic effect, the hydrogels of GEL(Au), GEL(AIPH) and GEL(Au+AIPH) were all selected to examine the cytotoxicity on 4T1 cells and MCF-7 cells under both normal oxygen concentration and hypoxia condition. As illustrated in Fig. 5A and 5B, the hydrogels showed nearly no dark cytotoxicity on 4T1 cells no matter the concentration of oxygen, demonstrating the good biocompatibility of the hydrogels. And the GEL (AIPH), which contained the only AIPH, but no AuNR, showed low cytotoxicity even under irradiation (785 nm, 1 W/cm^2,10 min) under normal oxygen concentration and hypoxia condition. Also for the GEL(Au), which contained AuNRs, but no AIPH, the cell viabilities were much lower, confirming the photothermal effect of the hydrogels. However, for the GEL(Au+AIPH), which contained both AuNRs and AIPH, exhibited lower cell viabilities than GEL(AIPH), indicating the obvious cytotoxicity effect to the cells by the generated free radicals of AIPH, further verifying the combination therapeutic effect of photothermal and thermodynamic therapy. Interestingly, no
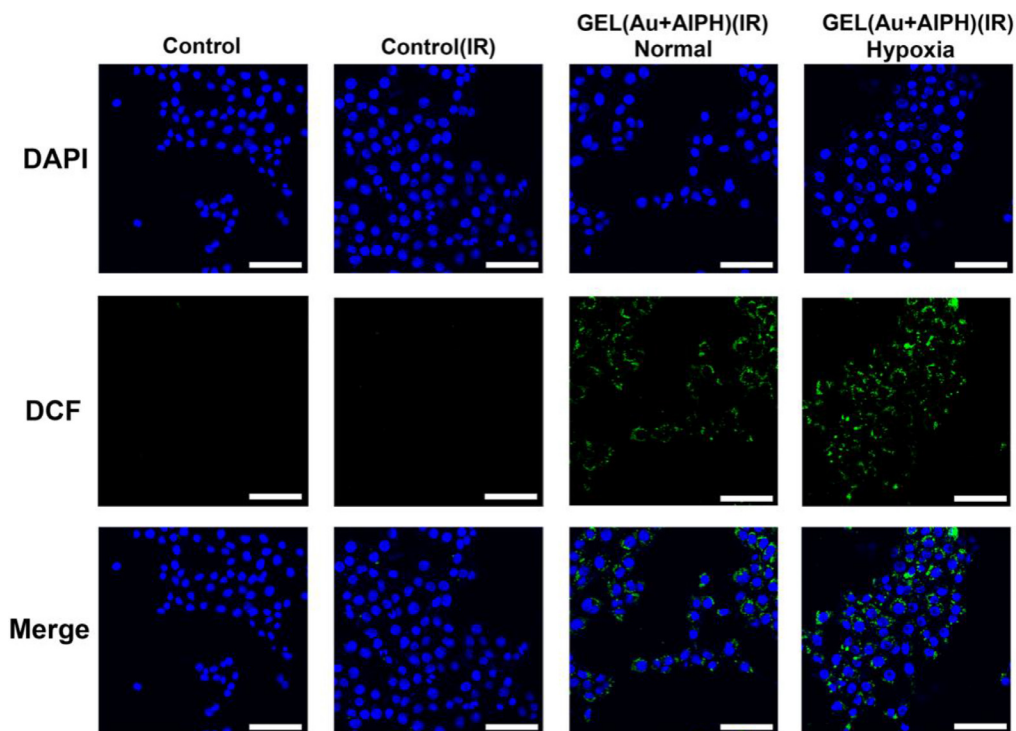
Fig. 6 – The confocal microscopy images of 4T1 cells treated with hydrogels with irradiation (785 nm, 1 W/cm^2,10 min) under normal oxygen concentration or hypoxia condition. The nucleus is stained with DAPI, and the green fluorescence corresponding to the radical probe of DCF. Scale bar: 50 μm. ($n = 3$). (For interpretation of the references to color in this figure legend, the reader is referred to the web version of this article.)
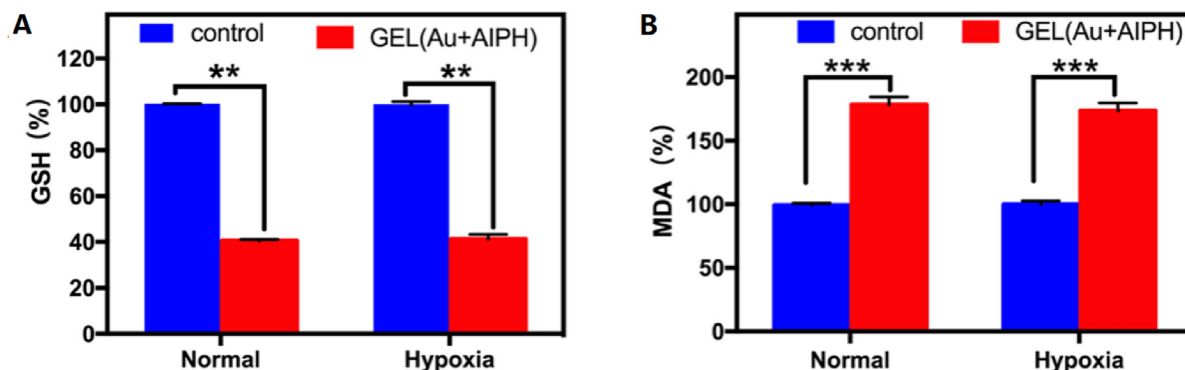

Fig. 7 – Intracellular level of GSH and MDA. (A) Intracellular GSH depletion of hydrogels with irradiation (785 nm, 1 W/cm^2, 10 min) under normal oxygen concentration or hypoxia condition. (B) Relative MDA content in 4T1 cells treated with hydrogels with irradiation (785 nm, 1 W/cm^2, 10 min) under normal oxygen concentration or hypoxia condition. Data are expressed as mean ± SD. ($n = 3$, **$P < 0.005$, ***$P < 0.0005$) .

significant difference could be observed for the influence of oxygen concentration on the cell viability. For the hypoxia groups, the culture medium was contained 100 μM CoCl$_2$ additionally, but there was no impact on the cytotoxicity of the hydrogels, which further verified that the generation of free radical of AIPH was not affected by the oxygen concentration. But for the PDT, the generation of ROS is oxygen-dependent, the therapeutic effect was diminished under the hypoxia condition. The similar results could be observed in MCF-7 cells shown in Fig. 5C and 5D, no evident cytotoxicity were observed to the hydrogels without irradiation and the laser irradiation

alone didn't cause additional damage to cells, proving the safety of the laser. GEL(Au+AIPH) exhibited the most effective cancer cells damaging, proving the generated free radicals could effectively kill the cancer cells. Also, the cytotoxicity of hydrogels was independent of oxygen concentration, because the free radicals of AIPH could be generated in the absence of oxygen, and the alkyl radicals could aggravate cell apoptosis even under oxygen pressure [12]. All these results presented the combination therapeutic effect of photothermal and thermodynamic therapy of the hydrogels even in the hypoxia condition.
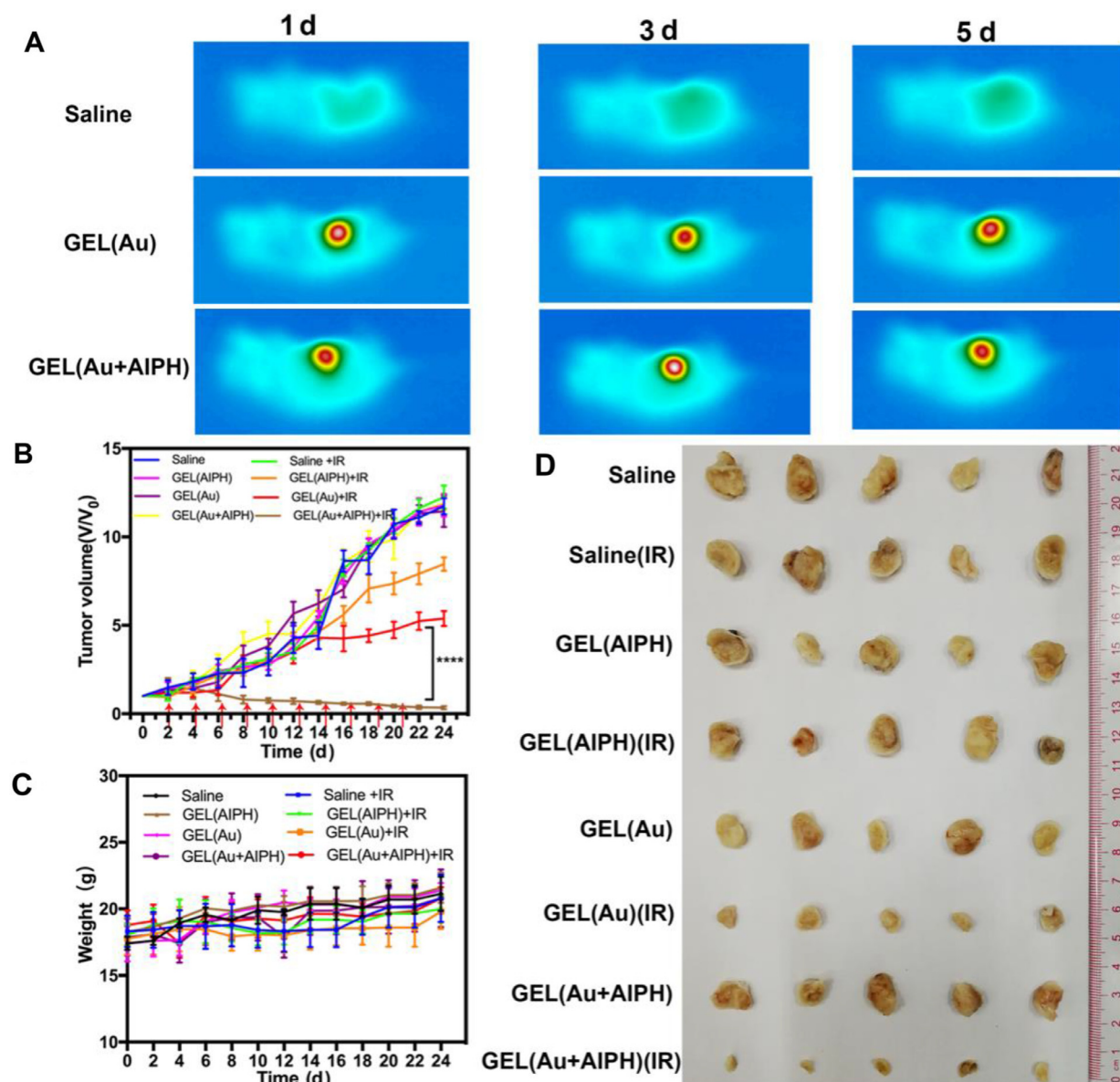
Fig. 8 – *In vivo* antitumor activity of different formulations in 4T1-bearing mice. (A) The IR thermal images of 4T1 tumor-bear mice with injected of Saline, GEL(Au) and GEL(Au+AIPH) under NIR laser irradiation (785 nm, 1 W/cm^2, 10 min) on Day 1,3 and 5. (B) Changes in relative tumor volume. (C) Average body weight of mice during therapy. (D) Photograph of the excised tumors after the mice were sacrificed on Day 24. Data are expressed as mean ± SD. ($n = 5$, ****$P < 0.0001$).

3.4.2. Intracellular free radical generation detection

Dichlorofluorescein diacetate (DCFH-DA) was employed to examine the generation of free radicals of AIPH intracellular in both normal oxygen concentration and hypoxia condition. Furthermore, it was thought that the alkyl radicals could be converted to the ROS by the intracellular oxygen under normoxia, inducing to a deep damage to cells. As shown in Fig. 6, 4T1 cells treated with GEL(Au+AIPH) exhibited bright florescence under NIR laser irradiation (785 nm, 1 W/cm^2, 10 min). Also, the green florescence under the hypoxia condition was observed as the similar intensity, further suggesting the free radicals could also be produced with low oxygen concentration under irradiation.

3.4.3. Intracellular depletion of glutathione and lipid peroxidation detection

Having proved the consumption of the GSH in the solution by the free radicals generated from the hydrogels, then, we verified the depletion of GSH intracellular by the commercial GSH assay kit. The relative GSH level were examined, for GEL(Au+AIPH), which could consume the GSH intracellular significantly shown in Fig. 7A, the relative GSH level could drop to 40.5% and 41.2% compared with the control group under normal oxygen concentration or hypoxic condition respectively, indicating the remarkable ability of GSH consumption by the hydrogels even in the absence of oxygen. Furthermore, MDA, served as the important
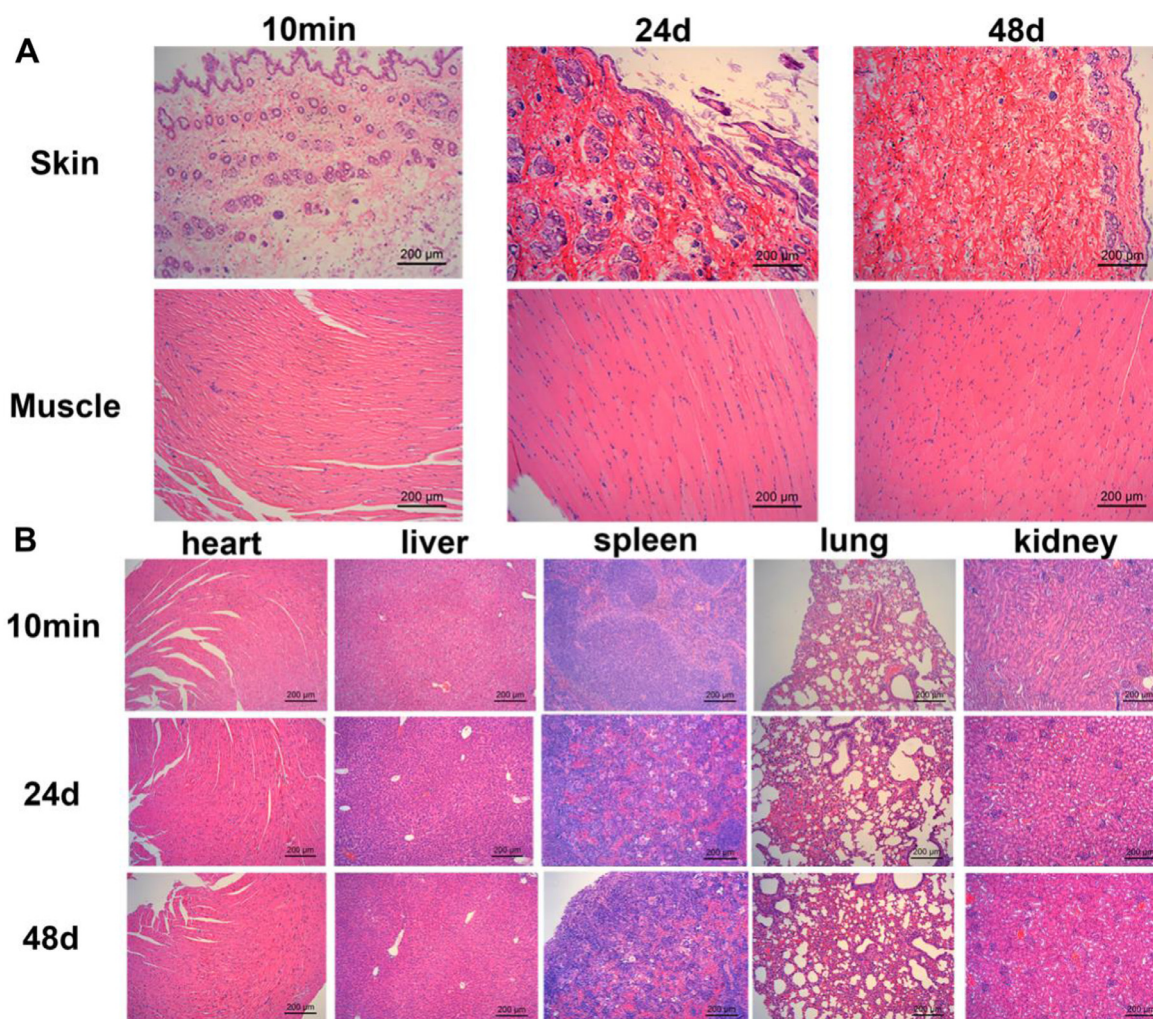
Fig. 9 – *In vivo* formation, degradation and biocompatibility of hydrogels. H&E staining of (A) Skin and muscle; (B) Other organs with the implanted hydrogel at 10 min after subcutaneous injection and Day 24 and 48.

intracellular lipid peroxidation marker, is an important product generated in the peroxidation process induced by free radicals. The relative intracellular MDA level were also tested to illustrate the lipid peroxidation, which would cause the damage to cells. When the hydrogels of GEL(Au+AIPH) employed on the 4T1 cells was exposed to the irradiation (785 nm, 1 W/cm^2, 10 min), more MDA would be produced through the peroxidation process compared with control. As demonstrated in Fig. 7B, upon on irradiation to GEL(Au+AIPH), the free radicals of AIPH were generated from the hydrogels, causing the lipid peroxidation and the elevation of relative MDA level to about 178.17% and 173.67% under normal oxygen concentration or hypoxia condition respectively, indicating the production of AIPH free radicals and result in the enhancement of the lipid peroxidation process independence of oxygen concentration.

3.5. *In vivo evaluations of hydrogels*

3.5.1. *In vivo IR thermal images of hydrogels*
To visualize the photothermal conversion effect of the hydrogels and ascertain the prolonged drug retention in the tumor region, the infrared (IR) thermal Images were carried out *in vivo*. As illustrated in Fig. S4, there was no obvious difference under irradiation for GEL(Au) and GEL(Au+AIPH), both of which contained AuNRs, resulting in a photothermal effect upon on irradiation. The temperature was rapidly increased to 45 °C, and nearly to 57 °C on the focus of laser after 10 min of irradiation, which was much higher than control group with saline. For the hydrogels of GEL(Au+AIPH), when the temperature was elevated, it was easy to induce hyperthermia, which could further trigger the generation of free radicals from AIPH, and induce the inhibition of tumor growth. Excitingly, the elevation of temperature of the hydrogels could also be observed on the 5th d after injection, as shown in Fig. 8A. The temperature in the tumor site could also increase to 45–55 °C on the 3th and 5th d of the hydrogels of GEL(Au) and GEL(Au+AIPH) upon the irradiation for 10 min, confirming the prolonged drug retention, which indicated that this hydrogel could be provided as a long-acting drug delivery carrier with a single dose.

3.5.2. *In vivo antitumor activity of hydrogels*
To investigate the *in vivo* antitumor efficiency by the combination effect of the photothermal and thermodynamic therapy, the BABL/C mice bearing 4T1 xenograft model were

established and injected with the corresponding solutions intratumorally, followed by the multiple rounds of irradiation at the 1, 3, 5, 7, 9, 11, 13,15,17 and 19 d The treatment effect was illustrated in Fig. 8, as expected, the hydrogels of GEL(Au), which contained the AuNRs, showed a PTT effect under the irradiation condition, which could partially suppress tumor growth in Fig. 8B and 8D. For the hydrogels of GEL(AIPH), contained the AIPH only, showed a slight inhibition efficiency under the irradiation compared with the control group of saline. Notably and importantly, while the hydrogels of GEL(Au+AIPH), contained both AuNRs and AIPH, exhibited the dramatically enhanced inhibition efficiency on tumor growth, suggesting the improved photothermal effect and the hydrogels could generate the free radicals *in vivo* for tumor therapy, further validating the combination effect of PTT and TDT even under the hypoxia condition in tumors. Besides, in Fig. 8C, there were no obvious changes on body weight of mice, indicating the negligible systemic toxicity during the treatment.

3.5.3. *In vivo formation, degradation and biocompatibility of hydrogels*

To confirm the quick formation of the hydrogels *in vivo,* the picture was taken to record the appearance of the hydrogels *in situ* after injection subcutaneously. As shown in Fig. S5, after injection for 10 min, the gelation was completely, validating the feasibility of gelation *in vivo*. And the gelation time *in vivo* was short to avoid the flow away of the precursor solution and diminish the toxicity. Also, it could be observed that the degradation of the hydrogel in Fig. S5, the size of the hydrogels was decreased with the time, in the 24th d, the size was nearly half of the size in 1st d, and in the 48th d, the hydrogel was almost completely degraded ultimately, which demonstrated the degradability of the hydrogel *in vivo*, due to the existence of hyaluronidase in subcutaneous tissues. To further verify the safety and the biocompatibility of the hydrogels, the H&E staining of the skin, muscle and the main tissues were established. As shown in Fig. 9, not only the instantaneously toxicities but also the long-term toxicities were not observed. There were no skin and muscle irritation of the hydrogels. No significant differences were found out in the pathologically histological tissue of skin and muscle at different time. Moreover, no systemic toxicity was observed in other tissues including heart, liver, spleen, lung and kidney even after degradation completely at 48 d, which illustrated the negligible toxicity of the monomers after degradation. All these results confirmed the good biocompatibility and safety of the hydrogels, which exhibited a promising long-acting delivery carrier.

4. Conclusions

In conclusion, we have established a NIR-triggered thermo-responsive long-acting hydrogels composed of HA-GMA and NIPAM, loaded with AuNRs and AIPH, which could combine PTT induced by AuNRs and TDT induced by free radicals. In this system, AuNRs, served as heat source, not only realized PTT but also could trigger the generation free radicals form AIPH and cause the shrink of hydrogel, which would accelerate the release of the free radicals upon the irradiation.

Compared with the photodynamic therapy, which was highly dependent on the oxygen, this new thermodynamic therapeutic strategy was an oxygen-independent and showed great advantages to the hypoxia tumor therapy. The results indicated that the hydrogels with a porous structure were exhibited a good mechanical property and an appropriated gelation time and showed a satisfied NIR-stimulated thermo-responsive properties. The intracellular evaluation confirmed the hydrogels exhibited significant inhibition effect on the growth of tumor cells under the normoxia and hypoxia condition. Meanwhile, the *in vivo* tests demonstrated the great antitumor activities and a prolonged drug retention, which could also realize the multiple treatments upon the repeated irradiation with single injection. Also, the hydrogel was biodegradable, which endowed the carrier good safety and biocompatibility. Therefore, this smart drug delivery system with the combination effect of photothermal and thermodynamic therapy showed a great potential for the hypoxic tumor therapy.

Conflicts of interest

The authors declare no competing financial interest.

Acknowledgments

Supplementary materials

Supplementary material associated with this article can be found, in the online version, at doi:10.1016/j.ajps.2019.11.007.

REFERENCES

[1] Luo T, Sun J, Zhu S, He J, Hao L, Xiao L, et al. Ultrasound-mediated destruction of oxygen and paclitaxel loaded dual-targeting microbubbles for intraperitoneal treatment of ovarian cancer xenografts. Cancer Lett 2017:3911.

[2] Bertout JA, Patel SA, Simon MC. The impact of O_2 availability on human cancer. Nat Rev Cancer 2008;8(12):967–75.

[3] Vaupel P, Hockel M, Mayer A. Detection and characterization of tumor hypoxia using pO2 histography. Antioxid Redox Signal 2007;9(8):1221–35.

[4] Zheng J, Shen Y, Xu Z, Yuan Z, He Y, Wei C, et al. Near-infrared off-on fluorescence probe activated by NTR for *in vivo* hypoxia imaging. Biosens Bioelectron 2018;119:141–8.

[5] Gao M, Liang C, Song X, Chen Q, Jin Q, Wang C. Erythrocyte-membrane-enveloped perfluorocarbon as nanoscale artificial red blood cells to relieve tumor hypoxia and enhance cancer radiotherapy. Adv Mater 2017;29(35):1701429.

[6] Han Y, Chen Z, Zhao H, Zha Z, Ke W, Wang Y, et al. Oxygen-independent combined

photothermal/photodynamic therapy delivered by tumor acidity-responsive polymeric micelles. J Control Rel 2018;284:15–25.

[7] Huang Z, Huang L, Huang Y, He Y, Sun X, Fu X, et al. Phthalocyanine-based coordination polymer nanoparticles for enhanced photodynamic therapy. Nanoscale 2017;9(41):15883–94.

[8] Cheng Y, Cheng H, Jiang C, Qiu X, Wang K, Huan W, et al. Perfluorocarbon nanoparticles enhance reactive oxygen levels and tumour growth inhibition in photodynamic therapy. Nat Commun 2015;6:8785.

[9] Liao W, Ning Z, Chen L, Wei Q, Yuan E, Yang J, et al. Intracellular antioxidant detoxifying effects of diosmetin on 2,2-azobis(2-amidinopropane) dihydrochloride (AAPH)-induced oxidative stress through inhibition of reactive oxygen species generation. J Agric Food Chem 2014;62(34):8648–54.

[10] Liu LH, Zhang YH, Qiu WX, Zhang L, Gao F, Li B, et al. Dual-stage light amplified photodynamic therapy against hypoxic tumor based on an O_2 self-sufficient nanoplatform. Small 2017;13(37):1701621.

[11] Zhu CH, Lu Y, Peng J, Chen JF, Yu SH. Photothermally sensitive poly(N-isopropylacrylamide)/graphene oxide nanocomposite hydrogels as remote light-controlled liquid microvalves. Adv Funct Mater 2012;22(19):4017–22.

[12] Chen ZH, Saito Y, Yoshida Y, Niki E. Effect of oxygen concentration on free radical-induced cytotoxicity. Biosci Biotechnol Biochem 2014;72(6):1491–7.

[13] Shen S, Zhu C, Huo D, Yang M, Xue J, Xia Y, et al. A hybrid nanomaterial for the controlled generation of free radicals and oxidative destruction of hypoxic cancer cells. Angew Chem Int Ed 2017;56(30):8801–4.

[14] Wang XQ, Gao F, Zhang XZ. Initiator-loaded gold nanocages as a light-induced free-radical generator for cancer therapy. Angew Chem Int Ed 2017;56(31):9029–33.

[15] Meng Z, Chao Y, Zhou X, Liang C, Liu J, Zhang R, et al. Near-infrared-triggered *in situ* gelation system for repeatedly enhanced photothermal brachytherapy with a single dose. ACS Nano 2018;12(9):9412–22.

[16] Xiang H, Lin H, Yu L, Chen Y. Hypoxia-irrelevant photonic thermodynamic cancer nanomedicine. ACS Nano 2019;13(2):2223–35.

[17] Wilhelm S, Tavares AJ, Dai Q, Ohta S, Audet J, Dvorak HF, et al. Analysis of nanoparticle delivery to tumours. Nat Rev Mater 2016;1:16014.

[18] Xu M, Mou YH, Hu MM, Dong WX, Su XT, Wu RX, et al. Evaluation of micelles incorporated into thermosensitive hydrogels for intratumoral delivery and controlled release of docetaxel: a dual approach for *in situ* treatment of tumors. Asian J Pharm Sci 2018;13(4):373–82.

[19] Annabi N, Tamayol A, Uquillas JA, Akbari M, Bertassoni LE, Cha C, et al. 25th anniversary article: rational design and applications of hydrogels in regenerative medicine. Adv Mater 2014;26(1):85–124.

[20] Wang C, Wang J, Zhang X, Yu S, Wen D, Hu Q, et al. In situ formed reactive oxygen species-responsive scaffold with gemcitabine and checkpoint inhibitor for combination therapy. Sci Transl Med 2018;10(429):eaan3682.

[21] Yu SJ, Wei S, Liu L, Qi DS, Wang JY, Chen GJ, et al. Enhanced local cancer therapy using a CA4P and CDDP co-loaded polypeptide gel depot. Biomater Sci 2019;7(3):860–6.

[22] Liu L, Gao Q, Lu XM, Zhou HF. In situ forming hydrogels based on chitosan for drug delivery and tissue regeneration. Asian J Pharm Sci 2016;11(6):673–83.

[23] Fu J, Wu B, Wei M, Huang Y, Zhou Y, Zhang Q, et al. Prussian blue nanosphere-embedded *in situ* hydrogel for photothermal therapy by peritumoral administration. Acta Pharm Sin B 2019;9(3):604–14.

[24] Xu X, Huang Z, Huang Z, Zhang X, He S, Sun X, et al. Injectable, NIR/pH-responsive nanocomposite hydrogel as long-acting implant for chemophotothermal synergistic cancer therapy. ACS Appl Mater Interfaces 2017;9(24):20361–75.

[25] Shi K, Liu Z, Wei YY, Wang W, Ju XJ, Xie R, et al. Near-infrared light-responsive poly(N-isopropylacrylamide)/graphene oxide nanocomposite hydrogels with ultrahigh tensibility. ACS Appl Mater Interfaces 2015;7(49):27289–98.

[26] Bencherif SA, Srinivasan A, Horkay F, Hollinger JO, Matyjaszewski K, Washburn NR. Influence of the degree of methacrylation on hyaluronic acid hydrogels properties. Biomaterials 2008;29(12):1739–49.

[27] Prata JE, Barth TA, Bencherif SA, Washburn NR. Complex fluids based on methacrylated hyaluronic acid. Biomacromolecules 2010;11(3):769–75.

[28] Liu H, Liu J, Qi C, Fang Y, Zhang L, Zhuo R, et al. Thermosensitive injectable in-situ forming carboxymethyl chitin hydrogel for three-dimensional cell culture. Acta Biomater 2016;35:35228–37.

[29] Wang B, Xu XD, Wang ZC, Cheng SX, Zhang XZ, Zhu RX. Synthesis and properties of pH and temperature sensitive P(NIPAAm-co-DMAEMA) hydrogels. Colloids Surf B 2008;64(1):34–41.

[30] Patterson J, Siew R, Herring SW, Lin ASP, Guldberg R, Stayton PS. Hyaluronic acid hydrogels with controlled degradation properties for oriented bone regeneration. Biomaterials 2010;31(26):6772–81.

[31] Takahashi A, Suzuki Y, Suhara T, Omichi K, Shimizu A, Hasegawa K, et al. In situ cross-linkable hydrogel of hyaluronan produced via copper-free click chemistry. Biomacromolecules 2013;14(10):3581–8.

[32] Mohring F, Jortzik E, Becker K. Comparison of methods probing the intracellular redox milieu in plasmodium falciparum. Mol Biochem Parasitol 2016;206(1–2):75–83.

[33] Becker K, Gui M, Traxler A, Kirsten C, Schirmer RH. Redox processes in malaria and other parasitic diseases: determination of intracellular glutathione. Histochemistry 1994;102(5):389–95.

[34] Liu Y, Zhen W, Jin L, Zhang S, Sun G, Zhang T, et al. All-in-One theranostic nanoagent with enhanced reactive oxygen species generation and modulating tumor microenvironment ability for effective tumor eradication. ACS Nano 2018;12(5):4886–93.

[35] Offor U, Naidu EC, Ogedengbe OO, Jegede AI, Peter AI, Azu OO. Nephrotoxicity and highly active antiretroviral therapy: mitigating action of Momordica charantia. Toxicol Rep 2018;5:51153–60.

[36] Yan B, Boyer J-C, Habault D, Branda NR, Zhao Y. Near infrared light triggered release of biomacromolecules from hydrogels loaded with upconversion nanoparticles. J Am Chem Soc 2012;134(40):16558–61.

[37] Strong LE, Dahotre SN, West JL. Hydrogel-nanoparticle composites for optically modulated cancer therapeutic delivery. J Control Rel 2014;178:17863–8.

[38] Li W, Wang J, Ren J, Qu X. 3D Graphene oxide-polymer hydrogel: near-Infrared light-triggered active scaffold for reversible cell capture and on-demand release. Adv Mater 2013;25(46):6737–43.

[39] Shiotani A, Akiyama Y, Kawano T, Niidome Y, Mori T, Katayama Y, et al. Active accumulation of gold nanorods in tumor in response to near-infrared laser irradiation. Bioconjugate Chem 2010;21(11):2049–54.

[40] Kesti M, Mueller M, Becher J, Schnabelrauch M, D'Este M, Eglin D, et al. A versatile bioink for three-dimensional printing of cellular scaffolds based on thermally and photo-triggered tandem gelation. Acta Biomater 2015;11:11162–72.